Slag Corrosion of Preceramic Paper Derived Multilayer Oxide Refractory

B. Gutbrod, N. Travitzky, A. Richter, M. Göbbels, P. Greil

Multilayer oxide ceramics of variable compositions were fabricated from preceramic paper to substitute carbon-bonded refractory. Alternating layers of ZrO_2, Al_2O_3–ZrO_2 and Al_2O_3–$MgAl_2O_4$ preceramic paper were bonded with a zirconia based interface adhesive layer and co-sintered at 1700 °C. The porous multilayer refractory structures were exposed to an industrial CaO–Fe_2O_3–SiO_2-slag melt at 1390 °C and the corrosion degradation mechanisms were analyzed. Progression of the corrosion zone is dominated by a layer-by-layer infiltration and dissolution reaction process. Zirconia laminates were found to exhibit superior corrosion resistance. Enhanced dissolution of interface layers was observed in the alumina-zirconia system. A pronounced volume expansion effect caused accelerated degradation in the alumina-spinel based system. ZrO_2 based interface bonding layers of lower porosity compared to the preceramic paper derived ceramic layers may improve corrosion resistance. Manufacturing of multilayer refractory structures from preceramic paper of various compositions offers high flexibility in stacking design optimization in order to adopt corrosion resistance to local environmental conditions.

1 Introduction

Refractories are used in a broad field of applications such as iron and non-iron metallurgy (70 %), glass-making, waste treatment and petrochemical refining [1]. During service they are generally exposed to elevated temperatures up to 2000 °C, thermal and/or mechanical stresses as well as corrosion attack by molten metal, silicate slags, salt fluxes and corrosive atmospheres [2–4]. The wide variety of desired functionalities lead to the development and application of a large variety of refractory compositions that are produced in numerous shapes and forms [1, 5]. Refractory components including for example shrouds, monoblock stoppers and submerged nozzles commonly consist of carbon-bonded materials, e.g. of MgO–C, Al_2O_3–C, ZrO_2–C, ZrO_2–CaO–C, Al_2O_3–SiO_2–SiC–C or Al_2O_3–SiO_2–C [6–10]. Fabrication often requires isostatic pressing of the oxide powder bonded by graphite loaded resin or pitch. Upon coking above 1000–1200 °C a carbon bond develops which increases the corrosion resistance in slag and metal melts, respectively. Furthermore, the carbon bond improves the thermo-mechanical properties, particularly the thermal shock resistance [6, 11].

Degradation of refractories is a complex phenomenon, which involves not only chemical wear (corrosion) but additional physical/mechanical wear (such as erosion/abrasion). When one of the phases involved is liquid, corrosion is often controlled by direct dissolution of the refractory with or without precipitation, by oxidation-reduction reactions between oxide and metallic elements or by complex reactions leading to the formation of new compounds [4]. In steel production, wear rate is often highest at the interface between slag and refractory lining. Most refractory materials have a certain amount of porosity which is not desired in terms of facilitated penetration of melt into the refractory microstructure. However, low porosity may increase susceptibility for thermal shock damage [3]. A certain amount of porosity, therefore, may improve refractory lifetime if penetration and corrosion are carefully controlled [2]. Theoretical aspects of chemical attack of solid refractories by liquid slags with emphasis on both penetration (simple permeation of liquid slag via open porosity) and reaction of the slag with the refractory phases are reviewed in [2]. Corrosion reactions during service of carbon-bonded refractories at elevated temperatures may involve the oxidation of the

Björn Gutbrod, Nahum Travitzky, Peter Greil
Department of Materials Science and Engineering (Glass and Ceramics) and Centre for Advanced Materials and Processes (ZMP)
University of Erlangen-Nürnberg
91058 Erlangen
Germany

Andreas Richter, Matthias Göbbels, Applied Mineralogy
GeoZentrum Nordbayern
University of Erlangen-Nürnberg
91054 Erlangen
Germany

Corresponding author: *Björn Gutbrod*
E-mail: bjoern.gutbrod@email.de

Keywords: preceramic paper, multi-layered refractories, slag corrosion

Received: 06.08.2012
Accepted: 14.08.2012

Tab. 1 Feedstock composition for preceramic paper processing (excluding water)

Specimen	Pulp Fibers [vol.-%]	Y-TZP Powder [vol.-%]	Mg-PSZ Powder [vol.-%]	Al_2O_3 Powder [vol.-%]	Al_2O_3-$MgAl_2O_4$ Powder [vol.-%]	Starch Derivatives [vol.-%]
P-Z	19	32	42	–	–	7
P-AZ	19	–	28	45	–	7
P-AS	19	–	–	45	28	7

carbon and evaporation of CO_2. Detailed reviews of carbon based refractories can be found in [5] and [11].

Preceramic paper offers a novel approach to manufacture lightweight and multilayer ceramics with tailored macro- and microscopic properties [12]. Since the strength of the green paper sheet is provided by the pulp fiber network versatile shaping technologies established in paper making industry can be applied. Thermal decomposition of the pulp template leaves a network of elongated pores with the volume fraction, size and orientation determined by the fiber template [12–15]. Multilayer stacks can easily be processed and offer a great variety of layer structure designs. A gradient porosity multilayer design may be favorable in order to increase thermal shock resistance in refractories or other ceramic materials [16]. Lamination of preceramic papers with different inorganic powder loading or the use of filled adhesives offers an elegant way for manufacturing of such multilayer laminate ceramics with or without alternating gradient or stepwise variation of composition and microstructure [12–15]. Furthermore, laminated object manufacturing may be applied for fabrication of components with complex 3D geometries [13].

In this work, multilayer oxide ceramics were fabricated from preceramic papers loaded with ZrO_2, Al_2O_3–ZrO_2 and Al_2O_3–$MgAl_2O_4$, respectively. Interface bonding was provided by a zirconia based adhesive layer. The corrosion behavior of the sintered laminates was examined by a static sessile drop test using a CaO–Fe_2O_3–SiO_2 slag in order to gain additional information with regard to optimal design of layered preceramic paper derived refractory structures.

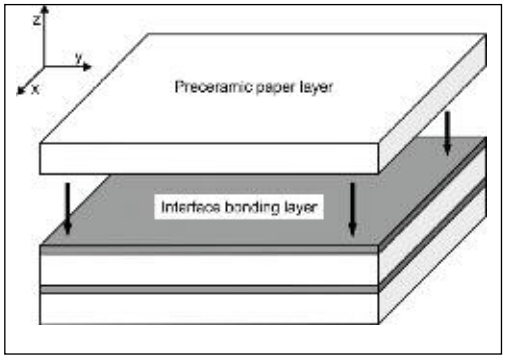

Fig. 1 Stacking of preceramic papers for the fabrication of multilayer refractories

2 Experimental procedure

2.1 Preceramic paper

Three different types of preceramic paper, loaded with 90, 86 and 84 mass-% mixtures of Y-TZP + Mg-PSZ (P-Z), Al_2O_3 + Mg-PSZ (P-AZ) and Al_2O_3 + Al_2O_3–$MgAl_2O_4$(P-AS) ceramic powders were prepared from aqueous suspensions. The pulp fiber and organic additives fraction was adjusted to 10, 14 and 16 mass-%. Organic additives were applied to control rheology and retention process. The aqueous suspension containing 0,6 vol.% non-refined hardwood pulp with an average diameter of 15 µm and an average length of 660 µm (Celbi PP, *Celulose Beira Industrial (Celbi) SA, Figueira da Foz*/PT) was homogenized by vigorous stirring at pH 7,6–8,1 for 1 h. 20 vol.-% aqueous suspensions of fine grained Y-TZP (CY3Z-MA, *Saint-Gobain Zirpro (Handan) Co. Ltd, Handan–Hebei*/CN) or Al_2O_3 (CT 3000 SG, *Almatis GmbH, Frankfurt*/DE) fillers with mean particle sizes of 0,2 µm and 0,5 µm, respectively, were added. Mg-PSZ (ZrO_2/MgO 97/3–15 µm, molten and ground, *Ceram GmbH Ingenieurkeramik, Albbruck-Birndorf*/DE) and Al_2O_3–$MgAl_2O_4$ (AR 78–20 µm, Almatis GmbH, Frankfurt/DE) fillers with mean particle sizes of 7,5 µm and 2,0 µm were added to the pulp suspension. Retention losses of the fillers were compensated by adequate amounts of excess filler. Flocculation of the feedstock suspension was induced by addition of 2 vol.-% cationic and 5 vol.-% anionic starch derivatives (Fibraffin K72 and Fibraffin A5, *Südstärke GmbH, Schrobenhausen*/DE). Tab. 1 summarizes the feedstock composition excluding water.

Preceramic paper sheets were formed on a Rapid Köthen sheet forming device (Haage Laborblattbildner BBS-2, *Estanit GmbH, Mühlheim an der Ruhr*/DE). Agitation of the diluted feedstock was achieved by pressing air through the suspension. Circular sheets with a diameter of 200 mm were obtained after dewatering applying a mild underpressure (<104 Pa). The as-filtrated specimens were dried at 93 °C for 15 min resulting in preceramic paper sheets (thereafter denoted as series P-Z, P-AZ and P-AS) with a medium thickness ranging from 215 µm to 295 µm.

2.2 Multilayer laminates

Multilayer laminates were fabricated by stacking up to 16 sheets. The sheets were bonded by a ceramic filler loaded adhesive suspension, Fig. 1. An aqueous dispersion of copolymerized polyvinyl acetate (Planatol AD 95, *Planatol Adhesive GmbH, Rohrdorf*/DE) loaded with 5,6 vol.-% Y-TZP (CY3Z-MA, Saint-Gobain Zirpro (Handan) Co. Ltd, Handan–Hebei/CN) and 6,9 vol.-% Mg-PSZ (ZrO_2/MgO 97/3–10 µm, molten and ground, *Ceram GmbH Ingenieurkeramik, Albbruck-Birndorf*/DE) with mean particle sizes of 0,2 µm and 5,8 µm, respectively, was stirred for 1 h and homogenized for 24 hours in a tumbling mixer (Turbula, *W.A. Bachhofen AG, Basel*/CH). The adhesive suspension contained 1,8 vol.-% aqueous Ammoniumpolymetacrylate suspension (Darvan C-N, *R.T. Vanderbilt Company Inc., Norwalk, Connecticut*/US) as dispersant, 16,7 vol.-% deionized water and 2 vol.-% of 1-Octanole (*Merck KGaA, Darmstadt*/DE) which serves as defoaming agent.

The laminates were debinded and sintered in air atmosphere in an electrically heated furnace (HT 16/17, *Nabertherm, Lilienthal*/DE). A single step annealing sequence was applied. The temperature was raised with a constant heating rate of 2,5–5 K/min up to 150 °C, followed by a heating rate of 0,5 K/min up to 350 °C. Temperature was held at 350 °C for 1 h followed by subsequent heating to 600 °C at 1 K/min. At 600 °C temperature was held for 1 h to assure complete removal of pulp and all organic additives. Laminates and sheets were

sintered at 1700 °C for 5 h. Heating from 600 °C to 1700 °C and cooling were performed at a rate of 5 K/min.

In-plane (parallel to the paper sheet) as well as out-of-plane (perpendicular to the sheet) shrinkage was measured. Mean *in-plane* areal shrinkage of the preceramic paper was measured by optical scanning (resolution 300 dpi) of rectangular specimens (40 mm × 40 mm) and subsequent image analysis to derive the specimen area (Image J V1.43, *Wayne Rasband National Institutes of Health, Bethesda, MD/*US). The linear shrinkage was calculated from the area assuming isotropic in-plane shrinkage. The out-of-plane shrinkage was measured by a micrometer screw with a resolution of 1 µm. Porosity and apparent density of the sintered ceramics were measured by water intrusion porosimetry (*Archimedes*). Microstructure of the multilayer laminates was derived from representative SEM micrographs (ESEM, Quanta 200, *FEI/*CZ) taken from cross-sections perpendicular to the sheet plane. The sintered specimens were embedded in epoxy resin and the cut surface was polished. Backscattered images showed a pronounced intensity difference between ceramic material and porosity, which allowed analysis of local porosity distribution.

2.3 Corrosion

Corrosion behavior was examined by static corrosion test (sessile drop test) with a pressed slag frit cylinder placed on the multilayer laminate specimens, heated to temperature and held for a fixed time period to allow slag to wet and react with the refractory. The slag composition (53 mass-% CaO, 30 mass-% Fe_2O_3, 8 mass-% SiO_2, 4 mass-% MnO and minor amounts of P_2O_5, MgO, Al_2O_3, TiO_2, Na_2O and K_2O) corresponds to a high basicity slag with a CaO/SiO_2 ratio of 6,6 and a melting temperature of 1375 °C as determined by DTA and TGA (STA 429, *Netzsch-Gerätebau GmbH, Selb/*DE).

Crystalline phases of the slag were determined by XRD-analysis (Kristalloflex D500, *Siemens, Mannheim/*DE) of powdered samples using monochromatic Cu-Kα radiation (λ = 0,154 nm). Total elementary composition of the slag was determined by ICP (Genesis, *Spectro Analytical Instruments GmbH, Kleve/*DE) after dissolving the powdered samples in $HF/HClO_4$ solution.

Tab. 2 Shrinkage, porosity and density upon sintering at 1700 °C for 5 h

Specimen	In-plane Shrinkage [%]	Out-of-plane Shrinkage [%]	Thickness [µm]	Porosity [%]	Density [g/cm³]
P-Z	19,5 ± 1,0	25,1 ± 2,7	221 ± 9	32,5 ± 3,0	3,71 ± 0,18
P-AZ	23,0 ± 0,2	27,1 ± 2,2	158 ± 3	30,9 ± 3,5	3,05 ± 0,18
P-AS	21,5 ± 0,3	29,0 ± 2,1	156 ± 4	27,1 ± 3,1	2,69 ± 0,09

Cylindrical slag samples with a diameter of 6 mm and a weight of 0,2 g were fabricated by uniaxial pressing of slag frit. The slag specimens were placed on the multilayer refractory samples and heated to 1390 °C in air in an electrically heated chamber furnace (HT 16/16, Nabertherm, Lilienthal/DE). A heating rate of 10 K/min was applied and the peak temperature was held for 1 h. After cool down, the samples were cut perpendicular to the slag/substrate interface, embedded in epoxy resin and polished. Slag infiltration depth and local reaction microstructure were analyzed by optical microscopy (Leica M420 and DC200, *Leica Microsystems Ltd, Heerbrugg/*CH), SEM (ESEM, Quanta 200, FEI/CZ), and EDX (INCA x-sight TV A3, *Oxford Instruments, High Wycombe/*GB). The chemical composition of all phases was analyzed by wavelength dispersive electron probe microanalysis (WDS-EPMA) employing a Jeol JXA-8200 (*Jeol Ltd., Tokyo/*JP). The electron beam was accelerated with 15 kV and the probe current was set to 15 nA. The measurement time of the peaks was 20 s and each background was measured 10 s. After background correction the intensities of characteristic x-ray lines were compared with those of standard materials (single phase oxides and metals). The oxygen content was calculated according to valence of the cations. The error of the WDS-EPMA measurement is assumed to be less than 1 mass-%.

Element distribution in the slag infiltration profiles was determined by EDX grid analysis with 100 µm and 40 µm distance of analyzed points in X-direction and Y-directions, respectively. Special care was taken to assure that each layer of the multilayer ceramics was investigated by at least one line of analysis points. Porosity distribution in the corroded samples was determined by image analysis from backscattered SEM micrographs (ImageJ V 1.43u, Wayne Rasband, National Institutes of Health, Bethesda, MD/US). Appropriate threshold values of grey values were selected to separate solid phases from porosity. A profile plot was derived representing the individual porosity of each line of pixels.

3 Results and discussion

3.1 Multilayer laminate manufacturing

Tab. 2 summarizes the sintering behavior and properties of the single preceramic paper sheets. A linear in-plane shrinkage of 19–23 % and a porosity of 25–35 % were observed in the single sheets with a thickness ranging from 150 µm to 330 µm. A zirconia powder filled adhesive layer with a thickness of approximately 50 µm (there-

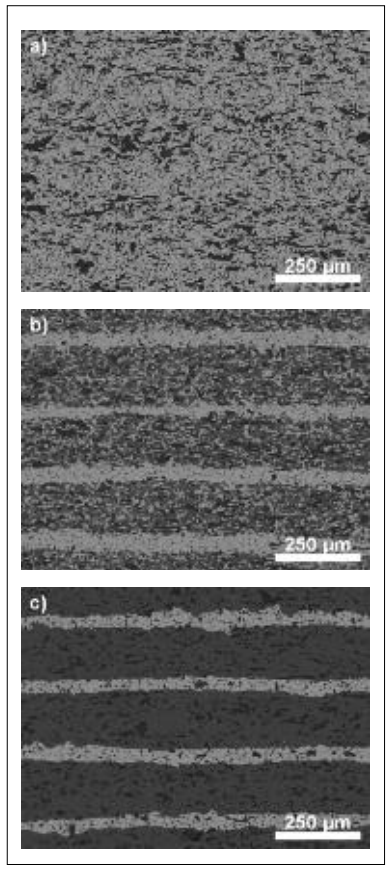

Fig. 2 Microstructure of sintered (1700 °C, 5 h) multilayer laminates derived from a) P-Z, b) P-AZ, c) P-AS, respectively, bonded with the zirconia loaded adhesive

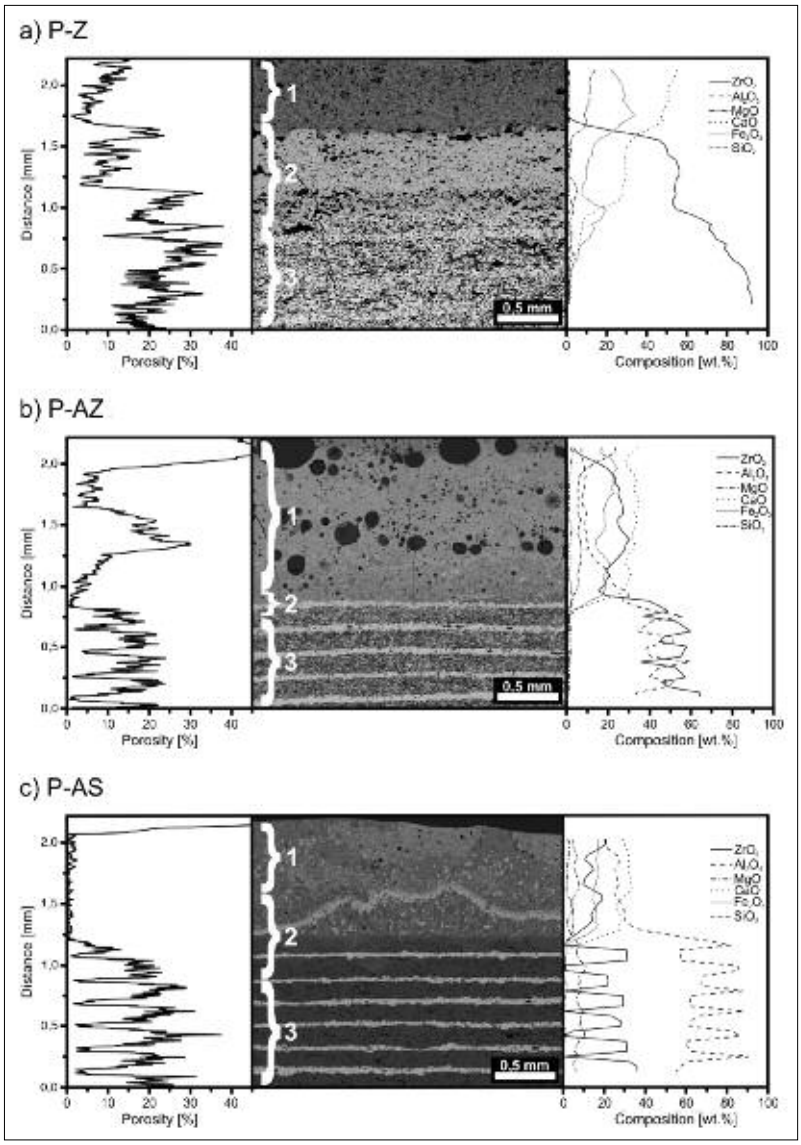

Fig. 3 a–c Porosity, slag infiltration behavior and element distribution of multilayer laminates derived from preceramic papers P-Z (a), P-AZ (b), and P-AS (c); microstructure of the laminates shows a slag region (1), a corrosion reaction zone (2), and the unreacted laminate material (3)

after called interface bonding layer) was applied to achieve lamination of the multilayer preceramic paper stack. Adapting the sintering shrinkage of the interface bonding layer and the ceramic sheet was achieved by mixing appropriate amounts of coarse-grained (low shrinkage) and fine-grained (high shrinkage) powders. Neither delamination nor crack patterns were observed in the multilayer stacks after sintering at 1700 °C for 5 (Fig. 2).

The macrostructures of the sintered laminates are characterized by a sequence of alternating layers of paper-derived oxide refractory layers and zirconia interface bonding layers. Image analyses of SEM micrographs indicate a sequential variation of porosity with low porosity interface bonding layers (5–10 %) separating refractory oxide layers of higher porosity (P-Z 30 %, P-PZ 20 %, P-AS 25 %). WDS-EPMA and XRD-analyses revealed the zirconia to consist of a mixture of monoclinic and tetragonal/cubic phase (e.g. partially stabilized zirconia).

3.2 Corrosion reactions

Fig. 3 a–c shows the microstructure, porosity and element distribution of the three different multilayer laminate compositions after exposure to slag melt at 1390 °C for 1 h.

The corrosion patterns of the microstructure may be separated into the slag region (1), the corrosion reaction zone (2) and the unreacted laminate material (3). Progress of the corrosion reaction zone follows a layer-by-layer mechanism as indicated by the characteristic variation of porosity and element distribution observed. Infiltration of the slag into the porous ceramic layers causes a reduction of porosity at the contact zone compared to the non-reacted laminate microstructure. EDX line scans reveal Zr concentration in the remaining slag to be almost negligible in the P-Z system, whereas slag melt in contact to the P-AZ and P-AS systems contained significantly higher Zr-concentrations up to 20 mass-%.

The total volume of corrosion reaction zone was derived from image analysis of cross-sections prepared perpendicular to the layer stacking, Fig. 4. Assuming ellipsoidal shape of the corrosion zone, values were determined from spreading diameter and penetration depth. The results indicate that resistance to corrosion degradation follows P-Z > P-AZ > P-AS. This may be expected from the solubility differences of the major ceramic constituents in the slag melt. For example, solubility of ZrO_2 in a calcia-sodia-silicate melt (SiO_2 40 mass-% – CaO 20 mass-% – Na_2O 20 mass-% – MgO 10 mass-% – Al_2O_3 10 mass-%) was found to be four times lower compared to Al_2O_3 and $MgAl_2O_4$ [17]. However, slag composition applied in this work is more basic characterized by a CaO/SiO_2 weight ratio of approximately 7, which was reported to favor dissolution of ZrO_2 [18]. Slow diffusional transport through the melt and precipitation of interface reaction products may give rise for slow reaction progress. Though the multicomponent composition of the slag melt causes a number of minor reaction products including ternary, quaternary and multicomponent solid solution phases to form in the contact zone between the melt and the ceramic, phase analyses suggest the following major reaction sequences to dominate:

P-Z $19\ ZrO_2 + 6\ CaO \rightarrow Ca_6Zr_{19}O_{44} + 13\ CaO \rightarrow 19\ CaZrO_3$ (1)

P-AZ $6\ Al_2O_3 + CaO \rightarrow CaAl_{12}O_{19} + 5\ CaO \rightarrow 6\ CaAl_2O_4$ (2)

P-AS $MgAl_2O_4 + 3\ CaO + 2\ SiO_2 \rightarrow CaAl_2O_4 + Ca_2MgSi_2O_7$ (3)

Reaction of dissolved ZrO_2 with CaO in the slag melt gives rise for precipitation of $Ca_6Zr_{19}O_{44}$ as intermediate and $CaZrO_3$ as final interface reaction products, respectively. The dissolution of Al_2O_3 leads to saturation of the slag with Al_2O_3 and calcium aluminates (e.g. CA_2) precipitate. Reaction of $MgAl_2O_4$ spinel may give rise for substitution of Mg and Al by Ca, Mn, and Fe from the slag and form complex spinels [19]. Furthermore, earth alkaline silicates such as solid solution melilite Ca_2 (Mg, Al, Fe) [(Al, Si) SiO_7] are likely to form as interface reaction products.

3.3 Microstructure and corrosion

Progression of corrosion zone into the refractory structure will be mainly governed by I.) infiltration of the slag melt into the porous ceramic layers, and II.) dissolution by chemical reaction at the contact interface [2]. In addition to the differences in material composition the corrosion degradation reactions will be strongly influenced by the residual porosity observed in preceramic paper derived oxide ceramics which results from low green body packing density and burn out of pulp fiber during sintering [12].

3.3.1 Infiltration and multilayer porosity

The porosity provides access for the slag melt to penetrate into the ceramic layers. For the case of laminar flow the penetration rate q ($q = 1/A\ dh/dt$ where A is the cross sectional area, h is the infiltration depth, and s is the time) of a slag melt into a porous refractory follows *Darcy*'s law [20]

$$q = -\frac{K}{\eta}\nabla p \qquad (4)$$

where K is the permeability, and η is the slag melt viscosity. The pressure gradient ∇p denotes the effective driving force. For the case of capillary pressure, an approximately one dimensional behaviour is given with $\nabla p =$ p/h and $p = 2\gamma cos\theta/r_p$ (with r_p the pore radius, γ is the surface tension, and θ the wetting angle). By integrating of equ. (4) the penetration depth h is expressed by $h = k^* s^{1/2}$ which shows that the penetration depth of slag melt is proportional to square root of time and the *Washburn* coefficient of penetration $k^* = (-4K\pi r_p \gamma cos\theta/\eta)^{1/2}$ (the elongated porosity of the preceramic paper derived ceramics is approximated by assumption of cylindrical pore shape (cross sectional area $A = \pi r_p^2$)). The permeability K scales with pore size r_p and porosity ϕ and for porous particle microstructure is commonly expressed by the *Kozeny-Carman* model [21]:

$$K = c\frac{r_p^{\,2}\phi^3}{(1-\phi)^2} \qquad (5)$$

The pore shape constant c is a function of surface area and tortuosity of the porosity. Flow rate for one dimensional flow perpendicular to layering, e.g. into z-direction, through a single layer of thickness t and permeability K is given by [22]

$$q = -\frac{K}{\eta}\frac{\Delta p}{t} \qquad (6)$$

For a laminate structure composed of n layers in series a common flow rate and cross sectional area causes a harmonic average of the permeability expressed by [23]

$$q = -\frac{1}{\eta}\frac{\Delta p}{\sum_{i=1}^{n}\left(\frac{t_i}{K_i}\right)} \qquad (7)$$

where t_i and K_i denote the individual thickness and permeability values of layer i. Since the flow rate in the multilayer laminate will be dominated by the lower permeability layers a variation of porosity in different layers is expected to have a pronounced impact on the slag melt infiltration rate. Values of residual open porosity of approximately 30 % (P-Z), 20 % (P-AZ), and 25 % (P-AS), respectively, were measured on the refractory ceramic layers bonded by an adhesive ZrO_2 layer of lower porosity (5–10 %). Assuming to a first approximation constant slag melt properties (γ, θ, η) and taking measured values of layer thickness and layer porosity the tentative flow rate reduction of ZrO_2 multilayer laminate was calculated from equ. (7). Fig. 5 shows the variation of normalized flow rate versus increasing thickness of the interface bonding layer for different values of initial porosity of $\phi^{ibl} = 0,1$ and 0,05 respectively. Compared to the single layer porous ceramic material of same total thickness the multilayer laminate is likely to exhibit a pronounced reduction of flow rate with increasing interface bonding to ceramic layer thickness ratio. Thus for a thickness ratio of the system under investigation of 0,2 a tentative reduction by one order of magnitude is predicted for interface bonding

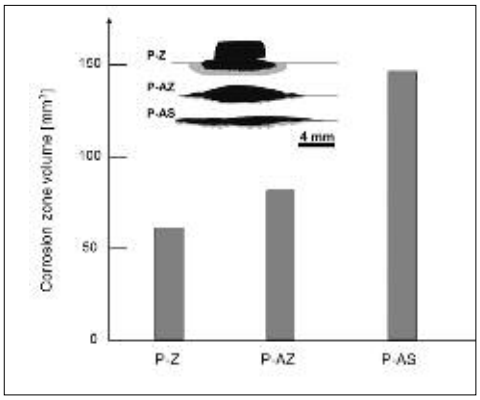

Fig. 4 Corroded volume and slag infiltration profiles of the preceramic paper derived multilayer laminates. Slag and corroded area are drawn in black, infiltrated and partially corroded area is gray; horizontal lines represent the laminate surface

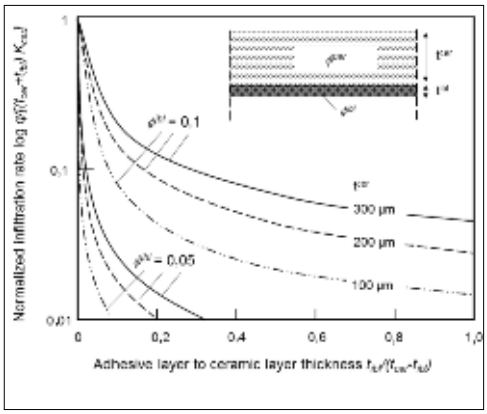

Fig. 5 Normalized flow rate calculated for different values of initial porosity of interface bonding layer (ibl), e.g. ϕ^{ibl} = 0,1 and 0,05, versus ibl-thickness

layer porosity of $\phi^{ibl} = 0,1$ and even two orders for $\phi^{ibl} = 0,05$.

3.3.2 Interface reaction and pore surface area

Dissolution controlled by interface reaction will be enhanced by increasing pore surface area. For dissolution to be controlled by a first order reaction the initial rate j may be expressed by [24]

$$j = kA_p\left(1 - \frac{\Pi_{ion}}{K_R}\right) \qquad (8)$$

k is the intrinsic rate coefficient, A_p the pore surface area which equals reaction surface area, and Π_{ion}/K_R quantifies the disequilibrium state of the melt/ceramic system (with

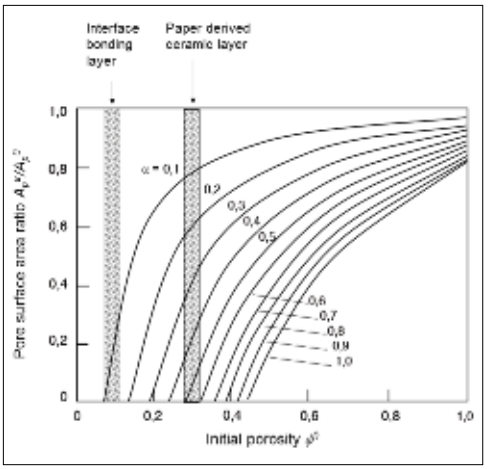

Fig. 6 Pore surface area reduction calculated for $\beta = 0{,}77$ (e.g. P-Z) for different values of degree of interface reaction versus initial porosity

Π_{ion} the ion activity product in the melt and K_R the equilibrium constant of the reaction under consideration). For direct dissolution to continue the atoms diffuse away from the interface into the slag melt at a rate proportional to $s^{1/2}$ as reactants are depleted and concentration of dissolved species increase accordingly (in the absence of melt convection or flow) [2]. Hence, porosity, which enhances the contact interface is expected to have a strong influence on the dissolution rate. Interface reactions between the infiltrating slag melt and the ceramic pore surface, however, may cause a solid volume expansion effect if the specific volume of the interface reaction product is larger than that of the ceramic skeleton phase. The volume expansion factor β may be expressed by

$$\beta = \frac{\Delta V}{V_s^0} = \frac{V_s^{ir}}{V_s^0} - 1 \qquad (9)$$

where V_s^0 is the initial solid volume (ZrO_2, Al_2O_3 and $MgAl_2O_4$ in equ. (1) – (3)), and V_s^{ir} is the volume of the interface reaction product ($CaZrO_3$, $CaAl_2O_4$, and $CaAl_2O_4$ + $Ca_2MgSi_2O_7$). The volume variation factor β derived for the idealized stoichiometric interface reactions (1) – (3) attain values of 0,77, 0,69 and 2,25 respectively. In the following ^{0} and ^{ir} denote initial and interface reaction product properties, respectively. In order to account for the degree of reaction α (e.g. $\alpha = 0$ no reaction, $\alpha = 1$ if all of the ceramics matrix phase has transformed to the reaction product), the volume variation factor is modified $\beta^* = \beta\,\alpha$. For the case of outer dimension of the porous ceramic layer structure to remain constant volume expansion associated with the interface reaction will be accommodated by a reduction of pore diameter and porosity

$$\frac{r_p^{ir}}{r_p^0} = (1 + \beta^*)^{1/3}$$

and

$$\frac{\phi^{ir}}{\phi^0} = 1 + \beta^* (1 - 1/\phi_0) \qquad (10)$$

Since the pore surface area A_p in a material section of volume V is dependent on porosity and pore size by

$$A_p = V \frac{m\phi}{r_p} \qquad (11)$$

where m denotes the pore shape constant (4–6) [24], the dissolution rate of interface controlled reaction is expected to scale with the variation of pore surface area by

$$\frac{j^{ir}}{j^0} \propto \frac{A_p^{ir}}{A_p^0} = \frac{1 + \beta^* (1 - 1/\phi^0)}{(1 + \beta^*)^{1/3}} \qquad (12)$$

Fig. 6 shows the tentative variation of the pore surface area versus degree of initial porosity in a preceramic paper derived multilayer laminate structure as calculated from equ. (12). The value of $\beta = 0{,}77$ applied in the calculation corresponds to the ZrO_2-multilayer material.

Though the calculation considers an idealized corrosion reaction model the results suggest the relation of porosity and interface reaction induced volume change to have a strong impact on the transport path and the reaction interface governing the corrosion reaction. Simultaneously to the reduction of infiltration rate the lower initial porosity level of the interface bonding layers ($\phi^{ibl} = 0{,}05$–$0{,}1$) compared to the preceramic paper derived ceramic layers is likely to retard interface controlled dissolution reaction during progression of corrosion zone. Independent on the specific material composition reduction of initial ceramic layer porosity as demonstrated previously [15] combined with interface bonding layers may offer a high potential for improving corrosion resistance of preceramic paper derived multilayer refractory ceramics.

4 Conclusions

Multilayer laminate structures derived from preceramic paper offer a high potential for manufacturing of refractory components with thermo-mechanical properties tailored by composition and layer microstructure. Reduction of porosity in the ceramic layer material is a key-factor in order to achieve improved corrosion resistance when exposing the multilayer ceramics to slag melt. Increasing of packing density in the starting preceramic paper precursor by improving the paper manufacturing as well as co-sintering process are envisaged in order to reduce porosity in microstructures of oxide based refractory materials. Compared to the single layer porous ceramic material of the same total thickness the multilayer laminate is likely to exhibit a pronounced reduction of slag melt penetration (flow) rate as well as interface controlled dissolution rate when an interface bonding layer of low porosity and high corrosion resistance based on ZrO_2 is applied. Hence, multilayer processing of preceramic paper derived ceramics offers a versatile approach to tailor microstructures such as alternating layer stacking and gradient variation of composition. Furthermore, low cost and well established shaping techniques of paper manufacturing may be applied.

Acknowledgements

Financial support from *DFG (p*riority programme FIRE) under contract number GR 961/31-1 is gratefully acknowledged. The authors would like to thank *Ingo Götschel* and *Prof Dr Andreas Roosen* from *University of Erlangen-Nuremberg*/DE as well as *Steffen Dudczig* and *Prof Dr Christos Aneziris* from *TU Bergakademie Freiberg*/DE for their cooperation.

References

[1] Banerjee, S.: Properties of refractories. In: Schacht, C.A. (editor): Refractories handbook. New York 2004, 1–10

[2] Lee, W.E.; Zhang, S.: Melt corrosion of oxide and oxide-carbon refractories. Int. Mater. Rev. 44 (1999) 77–104

[3] Brosnan, D.A.: Corrosion of refractories. In: Schacht, C.A. (editor): Refractories Handbook, New York 2004, 39–77

[4] Poirer, J.; et al.: An overview of refractory corrosion: observations, mechanisms and thermodynamic modeling. Refractories Applications Trans. 3 (2007) 2–12

[5] Lewis, G.: Refractories. In: Schneider Jr., S.J.

(volume chairman): Eng. Mater. Handbook, Vol. 4: Ceramics and Glasses. 2nd printing, Metals Park (OH) 2000, 895–909

[6] Aneziris, C.G.; Homola, F.; Borzov, D.: Material and process development of advanced refractories for innovative metal processing. Adv. Eng. Mater. 6 (2004) 562–568

[7] Leistner, H.; Ratcliffe, D.; Schuler, A.: Improved material design devices for continuous casting components. In: Proc. of the 2nd Worldwide Conf. on Refractories, Aachen 1991, 316–319

[8] Tsujino, R.; et al.: Mechanism of deposition of inclusion and metal in ZrO_2-CaO-C immersion nozzle of continuous casting. ISIJ Int. 34 (1994) 853–858

[9] Sasai, K.; Mizukami, Y.: Reaction mechanism between alumina graphite immersion nozzle and low carbon steel. ISIJ Int. 34 (1994) 802–809

[10] Sasai, K.; Mizukami, Y.: Reaction rate between alumina graphite immersion nozzle and low carbon steel. ISIJ Int. 35 (1995) 26–33

[11] Ewais, E.M.M.: Carbon based refractories. J. Ceram. Soc. Japan 112 (2004) 517–532

[12] Travitzky, N.; et al.: Preceramic paper-derived ceramics. J. Amer. Ceram. Soc. 91 (2008) 3477–3492

[13] Windsheimer, H.; et al.: Laminated object manufacturing of preceramic-paper-derived Si-SiC composites. Adv. Mater. 19 (2007) 4515–4519

[14] Gomes, C.M.; et al.: Preceramic paper derived fibrillar ceramics. Ceram. Trans. 210 (2010) 421–426

[15] Gutbrod, B.; et al.: Preceramic paper derived alumina/zirconia ceramics. Adv. Eng. Mater. 13 (2011) 494–501

[16] Hein, J.; Kuna, M.: Optimizing thermal shock resistance of layered refractories. Adv. Eng. Mater. 14 (2012) 408–415

[17] Fox, A.B.; et al.: Dissolution of ZrO_2, Al_2O_3, MgO and $MgAl_2O_4$ particles in a B_2O_3 containing commercial fluoride-free mould slag. ISIJ Int. 44 (2004) 836–845

[18] Chung, Y.-D.; Schlesinger, M.E.: Interaction of CaO-FeO-SiO_2 slags with partially stabilized zirconia. J. Amer. Ceram. Soc. 77 (1994) 611–616

[19] Korgul, P.; Wilson, D.R.; Lee, W.E.: Microstructural analysis of corroded alumina-spinel castable refractories. J. Europ. Ceram. Soc. 17 (1997) 77–84

[20] Scheidegger, A.E.: The physics of flow through porous media. Toronto 1974

[21] Carman, P.C.: Flow of gases through porous media. London 1956

[22] Barry, D.A.; Parker, J.C.: Approximations for solute transport through porous media with flow transverse to layering. Transport Porous Med. 2 (1987) 65–82

[23] Chen, Z.R.; Ye, L.; Liu, H.Y.: Effective permeabilities of multilayer fabric preforms in liquid composite moulding. Comp. Struct. 66 (2004) 351–357

[24] Lasaga, A.: Kinetic theory in the earth sciences. Princeton (NJ) 1998